Journal of ELECTRONIC MATERIALS, Vol. 49, No. 5, 2020
https://doi.org/10.1007/s11664-020-08023-y

Structural Phase Transformation, Intermediate States and Electronic Properties of PbTe Under High Pressure

HÜLYA ÖZTÜRK,[1,5] GÖZDE GÜL ARSLAN,[2] CİHAN KÜRKÇÜ,[3] and ÇAĞATAY YAMÇIÇIER[4]

1.—Department of Physics, Kırşehir Ahi Evran University, Kırşehir 40100, Turkey. 2.—Institute of Science, Kırşehir Ahi Evran University, Kırşehir 40100, Turkey. 3.—Department of Electronics and Automation, Kırşehir Ahi Evran University, Kırşehir 40100, Turkey. 4.—Institute of Science, Gazi University, Ankara 06500, Turkey. 5.—e-mail: hozturk@ahievran.edu.tr

In this work, density functional theory calculations in the framework of local density approximation (LDA) are performed using the Siesta software package in order to theoretically predict the phase transition mechanism and electronic properties of lead telluride (PbTe) under high hydrostatic pressure. PbTe undergoes a structural phase transformation from the cubic NaCl-type structure (B1) belongs to $Fm\bar{3}m$ space group to another cubic CsCl-type structure (B2) belongs to $Pm\bar{3}m$ space group with the influence of external pressure through the simulations. According to simulation results, we suggest a phase transition mechanism having four intermediate states with space groups of $P\bar{1}$, $C2/m$, $R\bar{3}m$ and $Cmmm$.

Key words: Lead telluride, high pressure, phase transformation, intermediate state, electronic properties

INTRODUCTION

Understanding of the electronic and structural properties of lead chalcogenides, Pb*X* (*X*; Te, Se, S), under pressure is important in the semiconductor device industry. These chalcogenides are narrow-gap semiconductors that are applied as sensors of infrared radiation, thermoelectric devices, photoresistors, lasers and other electronic devices.[1–4] During the last few decades, structural phase transitions in these chalcogenides under high pressure have attracted great interest.[5–9]

These materials crystallize in a cubic rock salt (B1) structure at ambient conditions. PbTe, one of the IV–VI compounds, is a semiconductor material with narrow and direct band transition. Because of these properties, it is widely used in technology for infrared devices.[10–13] Xu et al.[14] proved that B1 structure of PbTe was stable under mid-temperature to high temperatures and did not undergo a phase transition. However, according to their study, when pressure was applied to this B1 structure, it was observed that the structure changed into an orthorhombic structure with a space group, Pnma, distorted from this structure at approximately 6 GPa. They also proved that when the pressure continued to increase, at about 13 GPa, this orthorhombic structure started a second phase transformation into B2 structure and phase transformation was completed at 16 GPa. Bhambhani and Sharma also found that the cubic B1-type structure of PbTe was transformed into an orthorhombic B27-type structure under 6.77 GPa pressure. When they continued to apply pressure on this structure, they achieved phase transition to another cubic B2 type structure at 13.04 GPa.[15]

In experimental studies, there are difficulties in monitoring the changes in the positions of atoms and their movements during phase transition. In order to have a complete understanding of the physical properties of materials, the transition mechanisms are essential. Simulation works also allow these phase transformation mechanisms. Therefore, in this study, simulation works on structural and electronic properties of PbTe have been performed. In addition, one of the main origin points of this study is also four

(Received May 24, 2019; accepted February 13, 2020; published online February 25, 2020)

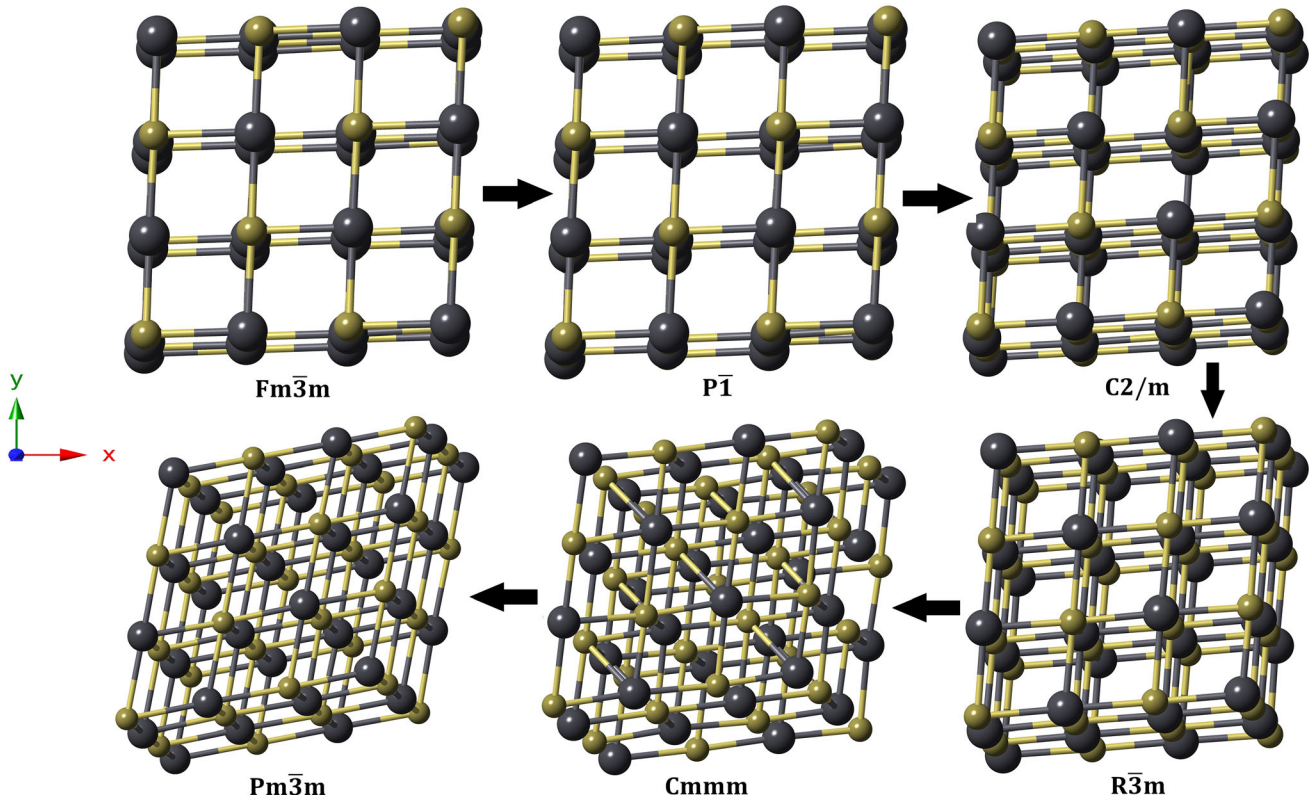

Fig. 1. (Color online) Evolution of the Pm$\bar{3}$m phase. All phases are viewed along [001] direction.

intermediate states. These intermediate states are P$\bar{1}$, C2/m, R$\bar{3}$m and Cmmm expressed as PbTe-(a), PbTe-(b), PbTe-(c), and PbTe-(d), respectively. It is also important to identify these intermediate states to understand the phase transition mechanism observed in PbTe under pressure. As far as we know, these intermediate states have not been obtained in any previous studies.

MATERIALS AND METHODS

The structural and electronic structure calculations were carried out within density functional theory (DFT) calculations using the Siesta software package.[16] Our calculations were performed using a local density approximation (LDA)-CA exchange–correlation functional.[17] There have been many attempts at obtaining accurate but approximate forms for the exchange–correlation functional for the ground state. The simplest of them, the LDA, gives a result which is very close to experimental results. In addition, LDA calculations are known for dramatic underestimations of band gap widths.[18,19] We have used Troullier-Martins type norm-conserving pseudo-potential for Pb and Te atoms.[20] All calculations were conducted using double-zeta plus polarized (DZP) basis sets of localized atomic orbitals. The energy mesh cut-off, which corresponds to the spacing of the real space grid used to calculate the Hartree, exchange, and correlation contribution to the total energy and Hamiltonian, was set to be 250 Rydberg (Ry). PbTe was modeled using $2 \times 2 \times 2$ cells with periodic boundary conditions for 64 atoms supercells. The Brillouin zones (BZ) were sampled with the $8 \times 8 \times 8$ Monkhorst–Pack k-point mesh.[21] Initially, structural optimizations such as lattice parameters, cut-off value, and atomic positions were performed via the conjugate-gradient (CG) method until the residual force acting on all atoms were smaller than 0.01 eV/Å and then pressure is gradually increased by an increment of 10 GPa through this method to the system. To analyze each minimization step, we used the KPLOT program and the RGS algorithm that give detailed information about the space groups, atomic positions and lattice parameters of an analyzed structure.[22,23]

RESULTS AND DISCUSSIONS

Firstly, PbTe is equilibrated by relaxing with 64 atoms supercell at zero pressure. The equilibrium unit cell lattice constants are found as $a = b = c = 6.4384$ Å for B1 structure of PbTe. We analyze the structure of this material at each applied pressure using the KPLOT program and obtain that the cubic NaCl-type structure belongs to Fm$\bar{3}$m symmetry is conserved up to 30 GPa. At this pressure, we observe the evolution of another cubic CsCl-type structure belongs to Pm$\bar{3}$m symmetry. The equilibrium unit cell lattice constants are found as $a = b = c = 3.6110$ Å for the CsCl-type structure.

Table I. Phase transition pressure value, lattice parameters, bulk modulus, and first derivative of bulk modulus for B1 and B2 structures of the PbTe compound

Structures	P_T(GPa)	$a = b = c$ (Å)	B_0(GPa)	B'_0	References
B1	0	6.4384	48.242	5.576	This Study
		6.4260	49.900	4.060	[28]
		6.5650	41.400	3.352	[29]
		6.3700	51.400	4.080	[29]
		6.4620			[30]
B2	6.4	3.6110	68.242	4.440	This Study
		3.8360	57.750	3.470	[28]
		3.9970	40.900	3.801	[29]
		3.8790	50.300	4.900	[29]

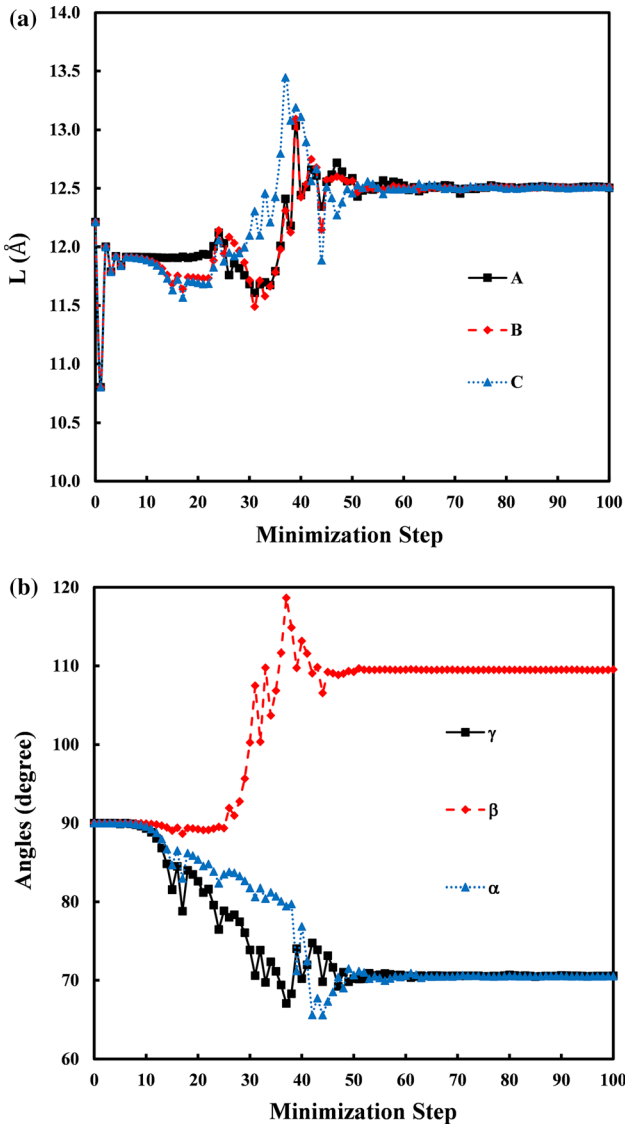

Fig. 2. (Color online) (a) The simulation cell lengths (L) and (b) angles as a function of the minimization step at 30 GPa for PbTe.

During the formation of the CsCl-type structure, each of the structures formed in the simulation steps was analyzed in detail using the KPLOT program. We observed four different intermediate states with space groups of $P\bar{1}$, C2/m, $R\bar{3}m$ and Cmmm. The crystal structures of B1, B2 and these intermediate states are illustrated in Fig. 1. Phase transition pressure value, lattice parameters, bulk modulus and first pressure derivative of bulk modulus for B1 and B2 structures are summarized in Table I with other studies in the literature.

To give details about the mechanism of phase transformation, simulation step dependence of the simulation cell vectors and angles should be examined. These cell vectors, expressed as **A**, **B**, and **C**, are initially along the [100], [010] and [001] directions, respectively. Figure 2a, b depicts the variation of the simulation cell lengths and angles as a function of minimization steps at 30 GPa. As shown in Fig. 2, small changes were observed in lengths A, B, and C up to approximately a 30th minimization step. After this step, the length of C increased to about the 40th minimization step. The lengths A and B decreased to about the 35th minimization step and then increased to the 40th minimization step. The lengths A, B and C then decreased to about the 45th minimization step and remained unchanged throughout the simulation.

The angles α, β and γ remained constant until the 10th minimization step. After this step, angle β increased to approximately 120° until the 40th minimization step, whereas the angles α and γ decreased until the 40th minimization step and reached about 65°. Then angle β decreased up to the 50th step and reached about 110°. After this step, there was not much change in angles α, β and γ and they remained almost constant throughout the simulation.

We have plotted the pressure–volume relation to determining the thermodynamic nature of the phase transition for PbTe in Fig. 3. We can infer

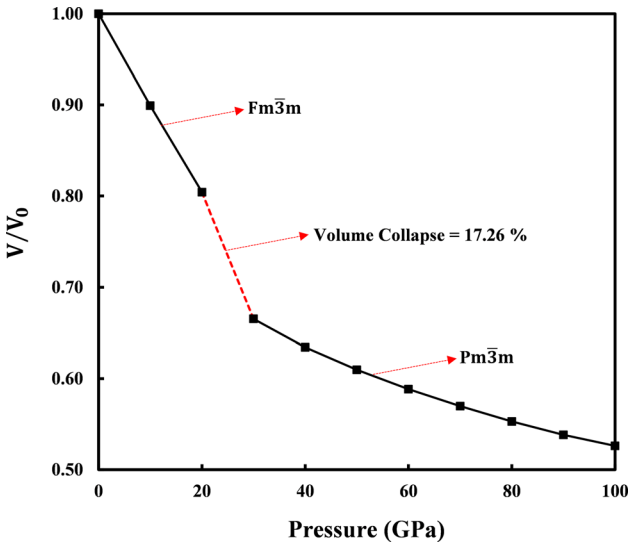

Fig. 3. (Color online) Volume-pressure relation of PbTe.

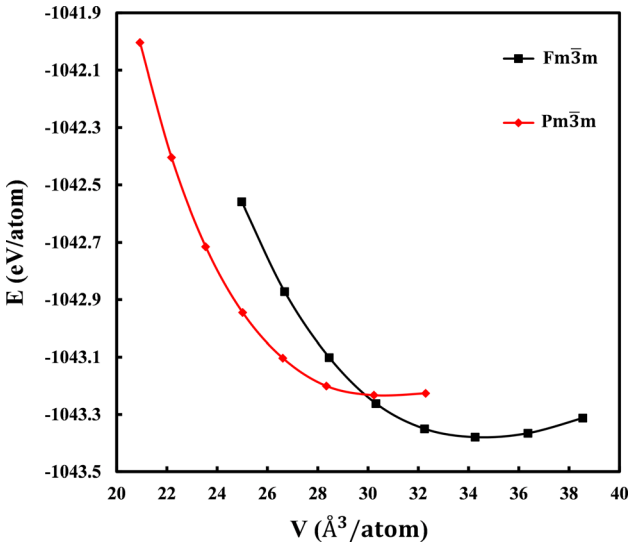

Fig. 4. (Color online) Energy-volume curves of PbTe for Fm3̄m and Pm3̄m phases.

that the volume decreases monotonically and shows a small discontinuity at 30 GPa. This discontinuity indicates the first-order phase transition. During this transition, volume collapse was observed at about 17.26%. As expected, the NaCl-type structure of PbTe transformed into the CsCl-type structure with space group Pm3̄m.

The transition pressure value obtained under hydrostatic pressure may be different compared to the transition pressure values obtained from other theoretical and experimental studies in the literature. The reasons for this are the limited size of the simulation cell, the fact that there may be defects in the real crystals, and neglecting the temperature effect. Because of the particular conditions, the transition pressure value can be overestimated.[24,25]

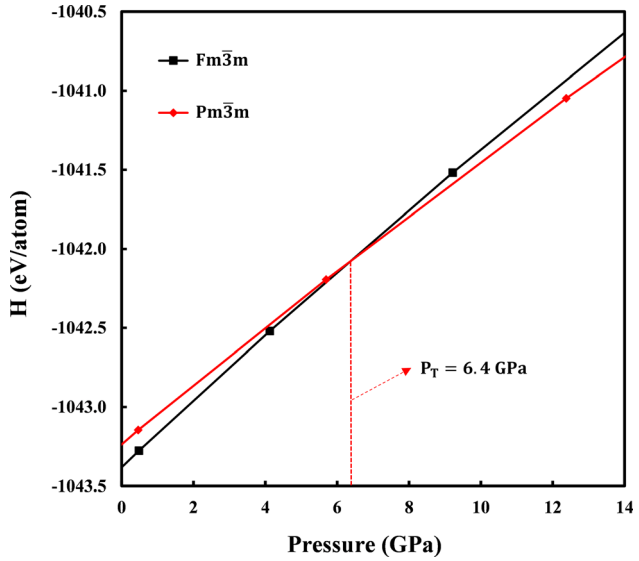

Fig. 5. (Color online) Enthalpy curves as a function of pressure for Fm3̄m and Pm3̄m phases of PbTe.

Energy-volume and enthalpy-pressure calculations will be made in the next step to obtain the closest result to the transition pressure values obtained from the other studies. In this way, we can obtain the most appropriate transition pressure value for this material.

We take the energy–volume computations into account to study the stability of the high-pressure phases of PbTe. For these calculations, we considered the unit cell for PbTe phases. The calculated total energy-volume relations are fitted to the 3rd order Birch-Murnaghan equation of state given in Eq. 1 and shown in Fig. 4.

$$P = 1.5B_0\left[\left(V/V_0\right)^{-7/3} - \left(V/V_0\right)^{-5/3}\right] x\left\{1 + 0.75(B_0' - 4)\left[\left(V/V_0\right)^{-2/3} - 1\right]\right\} \quad (1)$$

In Eq. 1, P, B_0, V/V_o and B_0', corresponds to the pressure, the bulk modulus, the volume ratio and the derivative of the bulk modulus, respectively.[26,27]

To determine which phase is thermodynamically stable at a given pressure and temperature, we used Gibbs free energy given as follows.

$$G = E_{\text{tot}} + PV - TS \quad (2)$$

In this equation, G, E_{tot}, P, V and S, correspond to Gibbs free energy, the total energy, pressure, volume and entropy, respectively. The "TS" term is neglected due to the calculations are carried out at the temperature of 0 K. Thus, G is equal to the enthalpy (H) given as below where $P = -\partial E_{\text{tot}}/\partial V$.

$$H = E_{\text{tot}} + PV \quad (3)$$

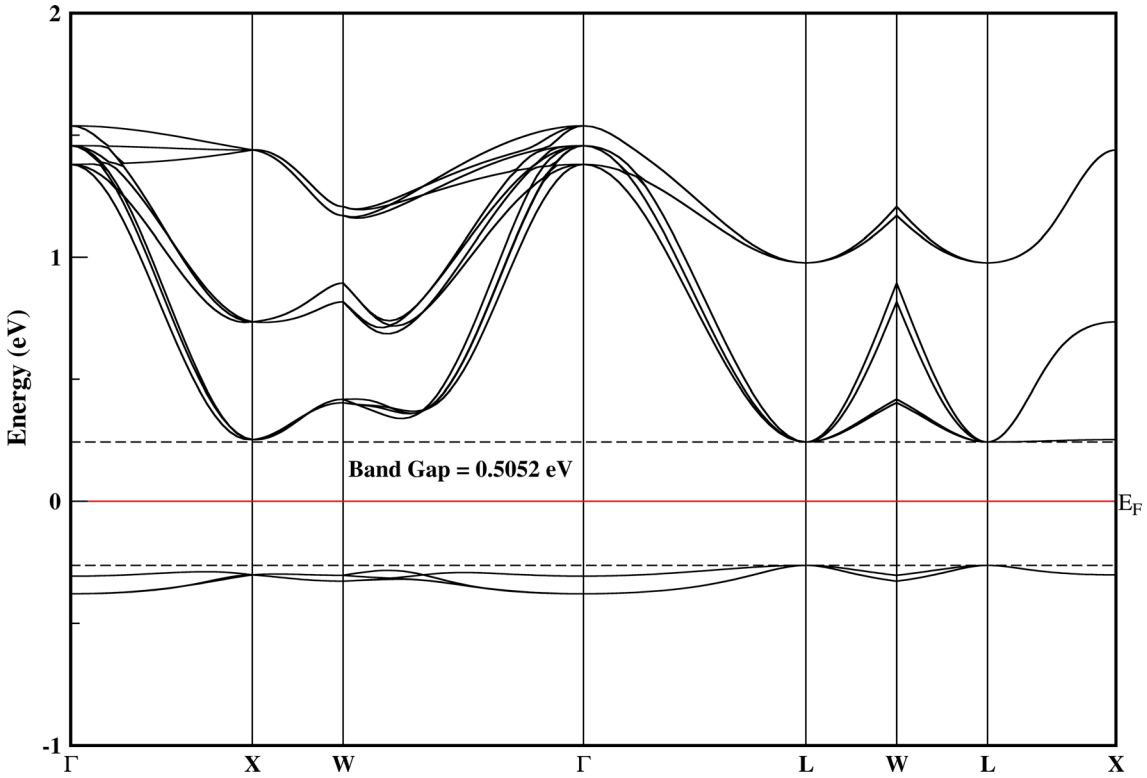

Fig. 6. Band structure for the Fm$\bar{3}$m phase of PbTe.

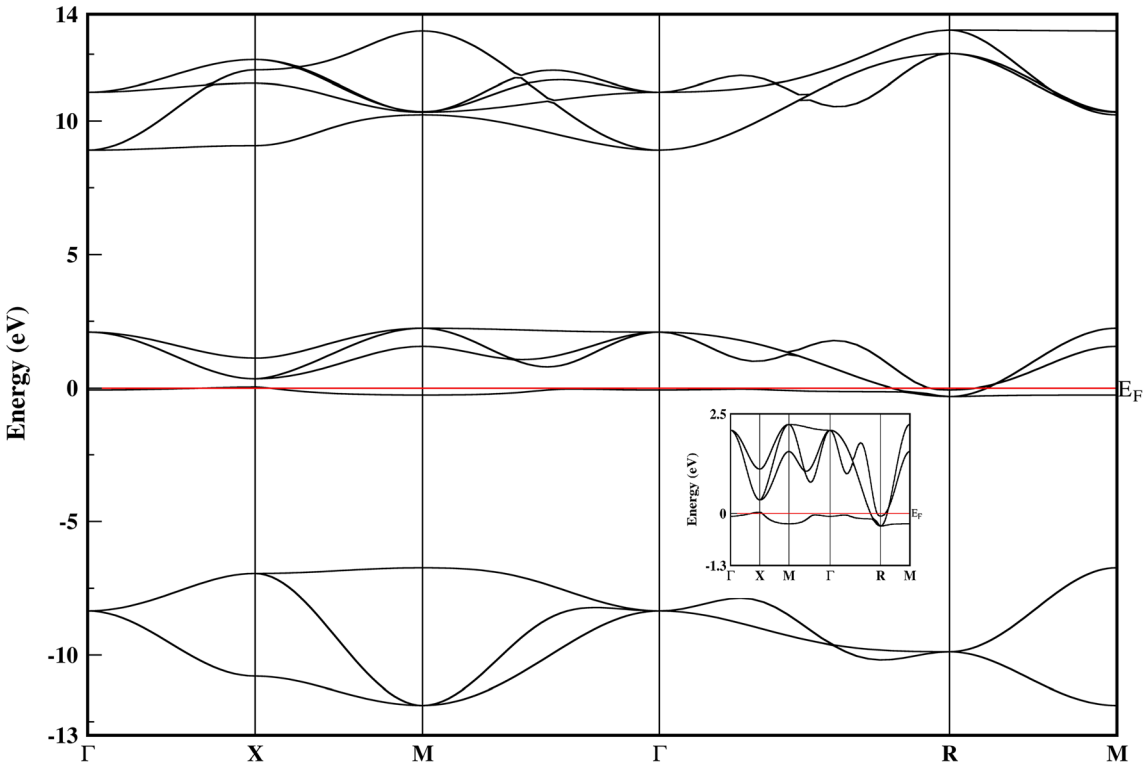

Fig. 7. Band structure for the Pm$\bar{3}$m phase of PbTe.

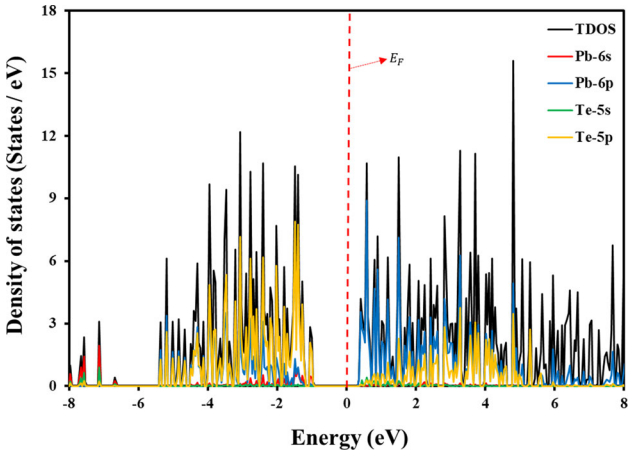

Fig. 8. The density of states for the Fm$\bar{3}$m phase of PbTe.

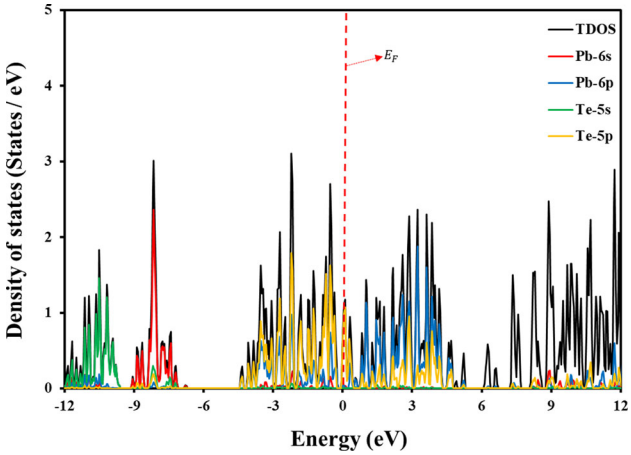

Fig. 9. The density of states for the Pm$\bar{3}$m phase of PbTe.

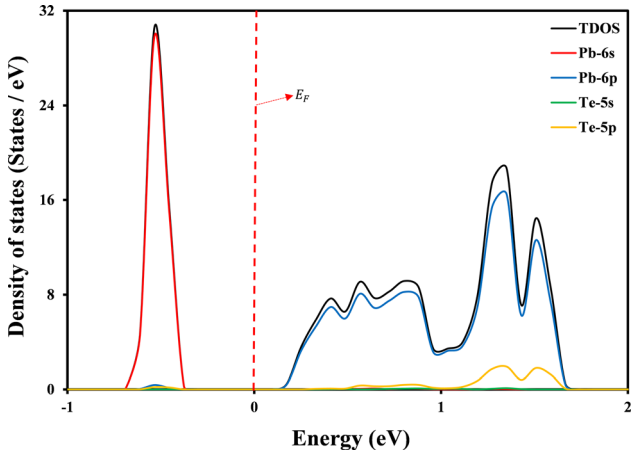

Fig. 10. The density of states for the Fm$\bar{3}$m phase of PbTe by using SOC.

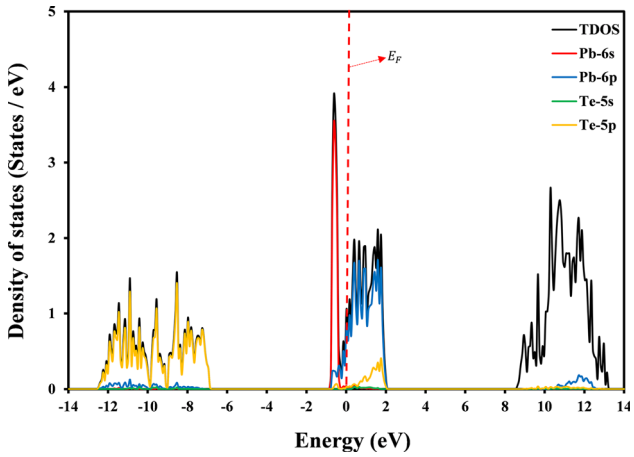

Fig. 11. The density of states for the Pm$\bar{3}$m phase of PbTe by using SOC.

Enthalpy calculations usually give transition pressure values close to the results obtained from experimental studies. The phase transition occurs when the enthalpies of the two phases are equal, that is, we use the thermodynamic criterion of equal free energies to predict accurate critical pressure. To determine the transition pressure, enthalpy curves are plotted as a function of pressure for NaCl-type structure and CsCl-type structure of PbTe and illustrated in Fig. 5. We can conclude from these curves that the phase transformation from the NaCl-type structure to the CsCl-type structure occurs at about 6.4 GPa.

We calculated the electronic band structures along with the high-symmetry directions using spin–orbit coupling (SOC), one of the scalar relativistic corrections, along with relativistic pseudopotentials and corresponding total and partial DOS as a function of energy for Fm$\bar{3}$m and Pm$\bar{3}$m phases of PbTe using non-relativistic and relativistic pseudopotentials. These are illustrated near the Fermi energy (E_F) level in Figs. 6, 7 for electronic band structure and Figs. 8, 9, 10, 11 for DOS, respectively. Fermi levels were set to be 0 eV. The symmetry points were $\Gamma - X - W - \Gamma - L - W - L - X$ for Fm$\bar{3}$m phase and $\Gamma - X - M - \Gamma - R - M$ for Pm$\bar{3}$m phase. According to Figs. 6, 7, Fm$\bar{3}$m phase of PbTe is a typical semiconductor, which exhibits a direct band gap with the energy of 0.5052 eV at the L-point of the Brillouin zone. On the other hand, Pm$\bar{3}$m phase of PbTe has no band gap at the Fermi level indicating the presence of metallic properties.

We calculated the partial DOS to obtain further information about the electronic nature of PbTe which is depicted in Figs. 8, 9 using non-relativistic pseudopotentials and in Figs. 10, 11 using SOC. As shown in Fig. 8, for theFm$\bar{3}$m phase, the largest contribution came from the Te-5p state between 0 and (− 6) eV and the Pb-6s state between − 6 and (− 8) eV below the Fermi energy level. Above the Fermi energy level, the biggest contribution came from the Pb-6p state between 0 and 8 eV. According to Fig. 9, for the Pm$\bar{3}$m phase, the largest

contribution came from the Te-5p between 0 and (− 6) eV, Pb-6s between − 6 and (− 9) eV and Te-5s between − 9 and (− 12) eV below the Fermi energy level. Above the Fermi energy level, the biggest contribution came from the Pb-6p state between 0 and 6 eV.

As shown in Fig. 10, for the $Fm\bar{3}m$ phase, the largest contribution came from the Pb-6s state below the Fermi energy level. The largest contribution came from the Pb-6p state above the Fermi energy level. According to Fig. 11, for the $Pm\bar{3}m$ phase, the largest contribution came from Pb-6s between (− 6) and 0 eV and Te-5p between (− 14) and (− 6) eV below the Fermi energy level. The largest contribution came from the Pb-6p state above the Fermi energy level.

CONCLUSION

In this work, ab initio calculations were performed to examine phase transition behavior of PbTe under high pressure with SIESTA. As a result of the calculations, a first-order phase transition was observed from the $Fm\bar{3}m$ phase to the $Pm\bar{3}m$ phase. In addition, four different intermediate states were predicted during this phase transition. These intermediate states were firstly predicted in this study. On the other hand, in order to better understand the physical properties of PbTe, electronic band structure and density of states were examined. Although the $Fm\bar{3}m$ phase of PbTe has a semiconductor character, it was observed that the high-pressure phase, $Pm\bar{3}m$ has a metallic character.

ACKNOWLEDGMENTS

This study was supported by the Kırşehir Ahi Evran University under Scientific Research Project (BAP) No: FEF.A4.16.002.

REFERENCES

1. D. Khokhlov, *Lead chalcogenides: physics and applications* (Boca Raton: CRC Press, 2002).
2. S.V. Ovsyannikov, V.V. Shchennikov, S.V. Popova, and A.Y. Derevskov, *Phys. Status Solidi B* 235, 521 (2003).
3. Y. Pei, A. LaLonde, S. Iwanaga, and G.J. Snyder, *Energy Environ. Sci.* 4, 2085 (2011).
4. S. Wang, J. Zhang, Y. Zhang, A. Alvarado, J. Attapattu, D. He, L. Wang, C. Chen, and Y. Zhao, *Inorg. Chem.* 52, 8638 (2013).
5. P. Bhambhani, K. Kabra, B.K. Sharma, and G. Sharma, *J. Solid State Phys.* 2014, 1 (2014).
6. T. Chattopadhyay, H.G. Von Schnering, W.A. Grosshans, and W.B. Holzapfel, *Physica B+C* 139, 356 (1986).
7. K. Hummer, A. Grüneis, and G. Kresse, *Phys. Rev. B* 75, 195211 (2007).
8. S.H. Wei and A. Zunger, *Phys. Rev. B* 55, 13605 (1997).
9. K.K. Zhuravlev, *Physica B: Condens. Matter* 394, 1 (2007).
10. T.K. Chaudhuri, *Int. J. Energy Res.* 16, 481 (1992).
11. A.F. Gibson, *Proc. Phys. Soc. B.* 65, 378 (1952).
12. H. Preier, *Appl. Phys.* 20, 189 (1979).
13. H. Zogg, A. Fach, C. Maissen, J. Masek, and S. Blunier, *Opt. Eng.* 33, 1440 (1994).
14. L. Xu, Y. Zheng, and J.C. Zheng, *Phys. Rev. B* 82, 195102 (2010).
15. P. Bhambhani and G. Sharma, *Ph. Transit.* 86, 551 (2013).
16. P. Ordejón, E. Artacho, and J.M. Soler, *Phys. Rev. B* 53, R10441 (1996).
17. D.M. Ceperley and B.J. Alder, *Phys. Rev. Lett.* 45, 566 (1980).
18. M. Rahaman, S. Ganguly, P. Samal, M.K. Harbola, T.S. Dasgupta, and A. Mookerjee, *Physica B Condens. Matter.* 404, 1137 (2009).
19. I.N. Yakovkin and P.A. Dowben, *Surf. Rev. Lett.* 14, 481 (2007).
20. N. Troullier and J.L. Martins, *Phys. Rev. B* 43, 1993 (1991).
21. H.J. Monkhorst and J.D. Pack, *Phys. Rev. B* 13, 5188 (1976).
22. R. Hundt, J.C. Schon, A. Hannemann, and M. Jansen, *J. Appl. Crystallogr.* 32, 413 (1999).
23. A. Hannemann, R. Hundt, J.C. Schon, and M. Jansen, *J. Appl. Crystallogr.* 31, 922 (1998).
24. H. Öztürk and M. Durandurdu, *J. Am. Ceram. Soc.* 94, 932 (2011).
25. H. Öztürk, C. Kürkçü, and C. Kürkçü, *J. Alloys Compd.* 597, 155 (2014).
26. F. Birch, *Phys. Rev.* 71, 809 (1947).
27. F.D. Murnaghan, *Proc. Natl. Acad. Sci. U.S.A.* 30, 244 (1944).
28. D.C. Gupta and I. Hamid, *Int. J. Mod. Phys.: Conf. Ser* 22, 612 (2013).
29. M. Lach-hab, D.A. Papaconstantopoulos, and M.J. Mehl, *J. Phys. Chem. Solids* 63, 833 (2002).
30. O. Madelung, *New Ser.* 17, 571 (1982).